Multiscale Full-Field Strain Measurements for Micromechanical Investigations of the Hydromechanical Behaviour of Clayey Rocks

Michel Bornert, Frédéric Valès, Houria Gharbi, D. Nguyen Minh

Multiscale Full-Field Strain Measurements for Micromechanical Investigations of the Hydromechanical Behaviour of Clayey Rocks

M. Bornert, F. Valès*, H. Gharbi and D. Nguyen Minh

Laboratoire de Mécanique des Solides, CNRS – UMR7649, Department of Mechanics, Ecole Polytechnique, 91128 Palaiseau, France

ABSTRACT: Digital image correlation techniques (DIC) are applied to sequences of optical images of argillaceous rock samples submitted to uniaxial compression at various saturation states at both the global centimetric scale of the samples and the local scale of their composite microstructure, made of a water-sensitive clay matrix and other mineral inclusions with a typical size of 50 lm. Various scales of heterogeneities are revealed by the optical technique. Not only is it confirmed that the clay matrix deforms much more than the other mineral inclusions, but it also appears that the deformation is very inhomogeneous in the matrix, with some areas almost not deformed, while others exhibit deformation twice the average overall strain (for a gauge length of 45 lm), depending on the local distribution of the inclusions. In almost-saturated rocks, overall heterogeneities are also linked to the presence of a network of cracks, induced by the preliminary hydric load. On such wet samples, DIC analysis shows that the overall strain results both from the bulk deformation of the sound rock, with deformation levels similar to those in dry samples, and the closing or opening of these mesoscopic cracks.

KEY WORDS: clayey rocks, cracks, digital image correlation, hydromechanical behaviour, multi-scale

Introduction

In the context of the underground nuclear waste disposal projects in deep argillaceous geological formations presently under investigation in France and in various other countries, many studies are focused on the characterisation of the thermo-hydro-mechanical behaviour of the rock in the neighbourhood of the repositories. This rock is subjected to various mechanical, hydrological, thermal and chemical aggressions during its life cycle, which may affect its stability and permeability. While most earlier studies were based on standard global rock mechanics characterisations [1], it is now acknowledged that reliable constitutive relations, required for medium- and long-term stability assessments, will require physically based micromechanical models, at all relevant scales of heterogeneity of such rocks, ranging from the nanometric scale of the clay layers to the kilometric scale of the geological formation. Such models require experimental investigations to identify the relevant micromechanisms to take into account and to validate their predictions at all scales. An important characteristic scale of heterogeneity of the Callovo-Oxfordian rocks from the French underground laboratory at Bure is linked to its composite structure. Indeed, this material is made of a clay matrix and various mineral inclusions (mostly carbonates and quartz), with sizes ranging from a few micrometres to a few hundred micrometres. This scale is of particular interest because the complex interactions between the water-sensitive matrix, which undergoes swelling or shrinkage depending on the surrounding atmosphere and exhibits plastic deformation, and the more rigid inclusions, may generate strong mechanical incompatibilities which are potential sources of damage. The present study, sponsored by ANDRA (the French agency for nuclear waste disposal) and CNRS (French national centre for scientific research), aims at characterising such heterogeneities at this microscale, and more generally detecting relevant centimetric to micrometric scales of heterogeneity, which would be the signatures of various active deformation and damage mechanisms. Attention is also focused on the influence of the water content of the material on these mechanisms.

*Present address: Laboratoire d'Ingénierie des Matériaux, Arts et Métiers ParisTech – CNRS, 151, boulevard de l'Hôpital, 75013 Paris, France

Such information will provide useful input and validation data for analytical or numerical micromechanical models currently under development [2, 3]. Because of the low deformation levels such rocks are able to sustain (about 2% overall strain at rupture, or less, depending on the hydric state), which do not permit direct microscopic observation of the micromechanism, full-field strain measurement techniques, used at both the centimetric scale of the sample and the micrometric scale of the composite structure of the rock, turn out to be pertinent tools for such investigations as presented hereafter.

The paper is organised as follows. The succeeding section is a short presentation of the tested material (origin and constitution) and the general experimental procedure, which combines imposed suctions to bring samples to a given degree of water saturation and uniaxial mechanical tests monitored both with standard measurement techniques and digital image correlation (DIC). The next section focuses on the optical setups used to investigate strain fields at macro- and microscales. Indications on the processing of the images and strain computations are also given, together with a discussion on the accuracy and possible sources of errors. The section *Selection of Results* is centred on the comparison of the mechanical response of an almost-dry [in equilibrium with an atmosphere at 44% relative humidity (RH)] and an almost-saturated sample (98% RH).

Materials and General Experimental Methodology

The indurated argillaceous rocks, or argillites, of the Bure site are well-compacted rocks from the Callovo-Oxfordian on the eastern part of the Paris basin. In this study, all samples were obtained from the same cell extracted at 481 m depth from the EST205 borehole. At this depth, the mineralogy reported in the literature [4] is typically characterised by a predominant clay fraction (45%), and grains of carbonates (20–28%), quartz (21–29%) and feldspar (0–4%); other minerals such as iron sulphur and organic material can be present, and the reported water content of the extracted rock is 8.5%. Our own systematic investigations of the tested material confirm most of these data, showing a total porosity of 16% (mercury intrusion porosimetry technique, performed on dried material and showing a dominant pore entrance diameter distribution ranging from 5 to 30 nm), a carbonate ratio of 27% (Bernard calcimetry technique) but a lower water content of 7%. The as-received rock was probably not saturated, a probable consequence of a slight desiccation during the after-sampling period. The unaided-eye observation of the samples shows a rather homogeneous texture, unlike what could be observed on other samples used in previous studies [5, 6]. The argillite shows a marked anisotropic texture [4] which induces transversely isotropic properties. Although the influence of this anisotropy on the global and local deformations has been addressed in this project [6], only results relative to compression tests normal to the sub-horizontal bedding are reported here.

Such overall petrophysical characterisations can be complemented by microstructural observations by scanning electron (SEM) and optical microscopy (OM) to identify the constitutive phases, characterise their spatial distributions and their typical sizes. Figure 1 shows SEM micrographs of a dry polished surface of a sample in the backscattered electron (BSE) mode. Argillite rock can be described as a composite structure with a continuous clay matrix and embedded mineral particles, essentially quartz and carbonates, which can be qualitatively distinguished by their grey

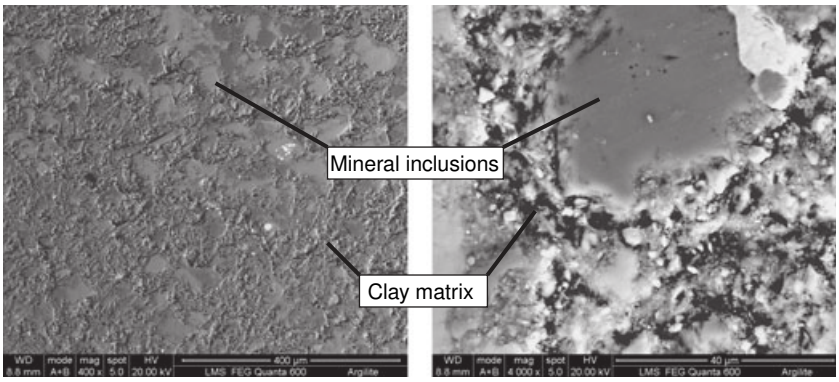

Figure 1: SEM micrographs at two magnifications of dry polished surface of indurated argillaceous rock; FEG ESEM FEI Quanta 600, backscattered electrons images, low vacuum mode. Calcite ($CaCO_3$) and quartz (SiO_2) grains appear in light and dark grey, respectively, white inclusions are pyrite framboïds (FeS_2). Fine structure of the clay matrix is seen in the higher resolution image (right)

level in BSE images or quantitavely analysed with energy-dispersive spectrometry [6]. The size of these particles ranges typically from a few micrometres to a few hundred micrometres, with an average close to 40 μm. They are rather homogeneously distributed in the matrix, but aggregates of several inclusions can be observed. A spreading of iron sulphur crystals is also observed, which appear white in the SEM images and are often associated with porosity. However, no significant porosity has been observed at this scale. This composite structure of the rock provides a natural contrast suited for the application of DIC technique at the macroscopic scale of the sample, as shown later. In addition, it can be seen in the high-resolution image in Figure 1 that the clay matrix itself exhibits a complex heterogeneous structure, with a typical length scale near or below a few micrometres, as clay is itself an aggregate of particles [4]. This scale of heterogeneity cannot be resolved by the DIC technique, but will serve to generate the appropriate contrast to measure strain within the clay matrix, considered as a continuous phase in the following.

We aim at providing a micromechanical insight into the hydromechanical behaviour of these rocks in order to develop and validate micromechanical models, taking into account the actual micromechanisms governing the overall behaviour. A first step includes identifying such mechanisms qualitatively by observation at relevant scales and quantifying their relative contributions. Multiscale strain-field measurement techniques, in particular those based on DIC, are efficient tools for such investigations, especially when the deformation levels are too small for a direct and systematic observation of the microstructure's evolutions. They have already been used for various studies on the elastoplastic behaviour of metallic single- or multiphase polycrystals (e.g. [7, 8]), using in particular *in situ* SEM tests for an improved spatial resolution. Their application to geomaterials is more recent with various problems: the smaller levels of deformation; the difficulty of applying an appropriate marking at the surface when the natural contrast is not sufficient; and often, the impossibility of using standard SEM imaging because vacuum conditions in the SEM chamber would dry out the samples and significantly modify their behaviour. This is in particular the case in the present study where we investigate the dependence with water content of the micromechanisms at the origin of the behaviour of the clayey rock. Such analyses at various hydric states are necessary to establish and validate physically based models for the hydromechanical behaviour of the rocks in the neighbourhood of underground repositories, where hydric conditions may undergo strong changes during the various stages of the service life of the repositories.

Towards that purpose, mechanical uniaxial compression tests are performed on cylindrical rock samples (36 mm in diameter and 72 mm in length) at various degrees of water saturation, from quasi-dry to quasi-saturated atmospheres. The deformation modes are characterised with optical observations and DIC techniques at various scales as detailed in the next section. Because of the very small depth of the field of OM and in order to limit the geometric aberrations of 2D DIC techniques, two flats in diametral opposition are machined and dry-polished up to paper grade 4000. Prior to the mechanical test, the samples are put in equilibrium with atmospheres whose RH is controlled using appropriate oversaturated saline solutions at constant temperature [1, 9]. The controlled suctions are 157, 113, 38 and 2.8 MPa, corresponding to RH values of 32%, 44%, 76% and 98%, respectively. During these purely hydric solicitations, which may last a few weeks, the changes in physical parameters (weight, longitudinal and transverse strains) are recorded continuously until stabilisation. In addition, microstructure evolutions can be observed at different scales, by comparing micrographs before and after the hydric load, with the help of DIC techniques when necessary and applicable; these results will not be detailed in the present paper. An important observation is however [6] that the as-received samples seem to be in equilibrium with an atmosphere at about 70% RH and are thus not saturated (consistent with the above-mentioned observation relative to the water content). Samples brought to lower degrees of saturation undergo an anisotropic shrinkage. A small – but clearly evidenced by image comparison – contribution to this overall shrinkage is linked to the closing of a few preexisting cracks, centimetric in size. Samples in equilibrium at 98% RH swell and a significant contribution to this swelling can be shown to be due to the opening of these cracks and the creation of new cracks. As shown later, these cracks contribute significantly to the overall mechanical behaviour of these materials in their wet state.

Uniaxial mechanical tests are performed in room conditions by using an electromechanical machine (Instron France S.A.S, Élancourt, France) with a low vibration level at a constant speed of 0.2 mm min^{-1} and monitored with classical overall sensors: load cell, displacement sensor [linear voltage displacement transducer (LVDT)] and 5×10 mm^2 strain gauges in longitudinal and transverse orientation. Optical images are recorded continuously as described hereafter. Note that the various strain measurement techniques involved exhibit a rather large range of gauge lengths:

decimetric for the LVDT sensor; centimetric for the strain gauges; and millimetric to centimetric for the overall DIC technique and ranging from 40 μm to 1.5 mm for the microscopic DIC procedure. This allows a multiscale detection of active mechanisms through the strain heterogeneities they generate, without any *a priori* assumption on the relevant scales. In addition, four piezoelectric transducers record acoustic events and allow one to localise their sources along the sample axis with a centimetric resolution.

Each test, performed up to the rupture of the sample, lasts a few minutes and the preparation time is of similar duration. This time is very short with respect to the duration of the suctions so that the overall water content of the sample can be considered as constant during the compression test. This is confirmed by the measurement of the water content of the debris. However, as the surface of the sample is in contact with the ambient atmosphere whose RH might be different from that of the sample, one cannot exclude that a thin outer layer of the material would swell or shrink during the test because of water exchange. The optical full-field measurements performed at the surface might therefore not be representative of the deformations in the bulk. Although we do not yet have a definitive answer to this question, the following arguments suggest that such artefacts might not be critical. First, we did not observe any qualitative evolution of the aspect of the surface of the sample, at both global and local scales. Secondly, several images were recorded during the setup, before any mechanical load was applied to the sample and their comparison by DIC techniques did not show any detectable deformation, while the application of the load clearly induced an evolution; the possible hydric deformations are thus probably negligible with respect to the mechanical deformations. A final answer to this question will be provided by performing the mechanical test within an environmental box with controlled atmosphere and temperature, compatible with the optical observations. This has not been done yet but is under development, especially in view of monitoring long-term deformations during creep tests.

Before describing in detail the optical setup used in the present study, let us emphasise that DIC techniques have been preferred to other optical full-field techniques because of their ease of use, the simplicity of the preparation of the samples and the direct observation of the sample surface. Speckle interferometric techniques could have been used and might have lead to more accurate results at the macroscale, but at the cost of a more complicated setup, which would probably hardly fit into the environmental box mentioned above. For investigations at the microscale, the resolution, limited by the wavelength of the light, would not have been significantly better than that of our DIC setup.

Optical Setup, Image Processing and Metrological Performances

Optical setup for macroscopic strain measurement 'MacroDIC'

A rather standard optical setup is used to record continuously images of the whole sample at a typical rate of 0.5 Hz. It consists of a 2/3-in. C-mount A101f progressive scan camera (Basler AG, Ahrensburg, Germany) which delivers $1300 \times 1030 \times 8$ bit images through its digital camera (DCAM) interface to a laptop computer running an in-house-developed acquisition software (DcamAqX) on a Linux operating system. A 90 mm Apo-Componon lens (Schneider-Kreuznach, Bad-Kreuznach, Germany) equipped with appropriate extension tubes (Unifoc 12 Makro-System; Schneider-Kreuznach) provides an optical magnification of about 1/8 to fit the sample height to the 8.7-mm-wide charge-coupled device (CCD) sensor (pixel size = 6.7 μm), so that the physical size of a pixel is about 52 μm. This is enough to resolve the larger quartz or calcite constitutive grains of the material, which provide a natural contrast which is sufficient, though not optimal, for a DIC analysis at the global scale of the sample. Note that in this configuration the distance from the surface of the sample to the optical centre of the lens is 81 cm. The sample is illuminated with a 112-mm-diameter ring light combined with a halogen incandescent light source, about 15 cm away from the sample. In order to avoid specular reflection on the sample, polarising filters are placed in front of the ring light and the lens in the extinguishing mode. The left-hand side of Figure 2 provides a general description of the setup and an example of the image obtained. It is noted that the available contrast is not optimal as the obtained grey-level histogram is rather narrow and the characteristic size of the patterns is small, as revealed by the radius of the normalised centred autocorrelation function (see Ref. [10] for the definition adopted) at half height below 2 pixels.

Optical setup for strain measurement at microscale 'MicroDIC'

Images at the smaller scale are recorded by means of a specifically designed optical microscope (see right-hand side of Figure 2), consisting of a Mitutoyo

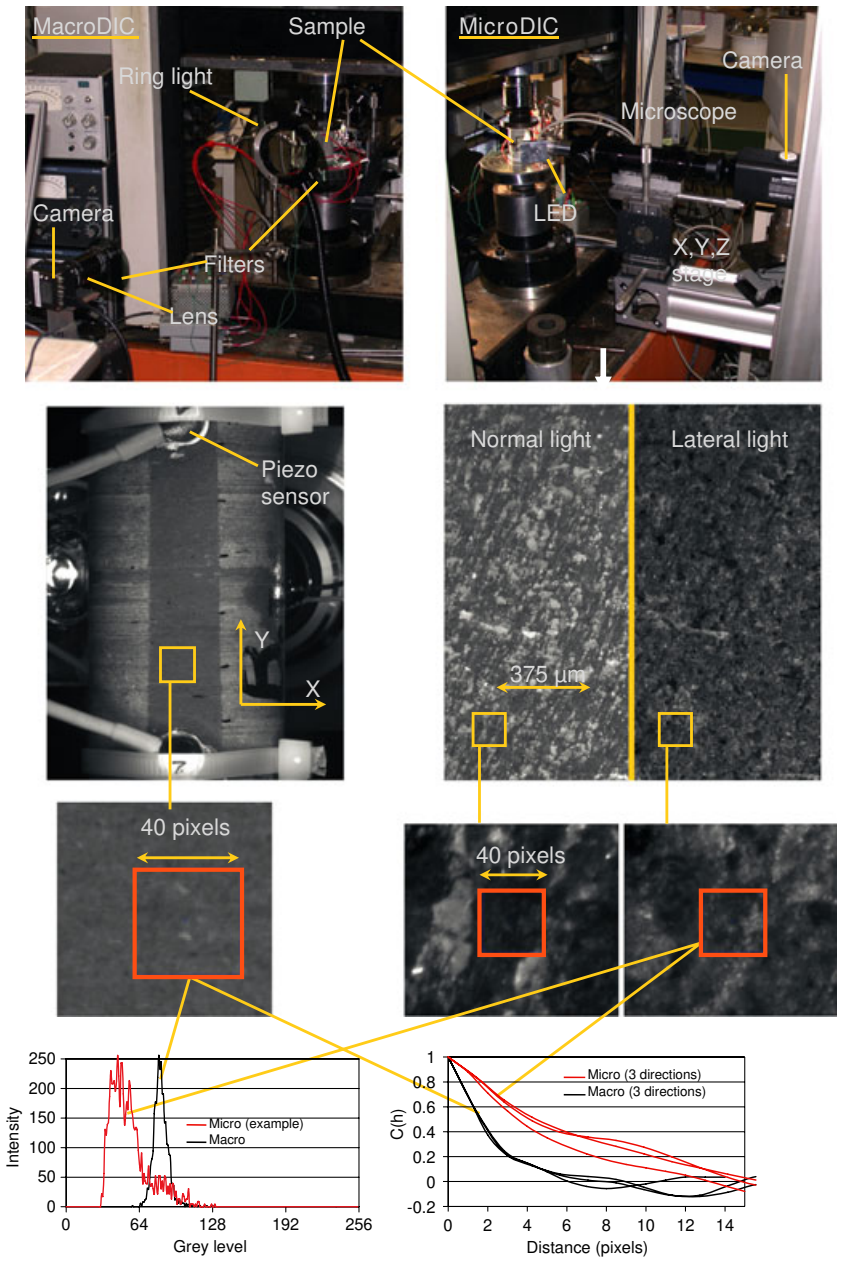

Figure 2: Description of the optical setups. Left: macroscopic scale, Right: microscopic scale. Top: experimental setup. Middle: examples of images (half images of same zone for microscopic scale, with normal and lateral lighting). Bottom: zooms on images and image characteristics (grey-level histogram and normalised autocorrelation function of typical 40 · 40 pixel subset)

infinity-corrected apochromatic 10 × objective lens with a working distance of 34 mm and a numerical aperture of 0.28, adapted to a C-mount Diagnostic Instrument (Sterling Heights, MI, USA) Spot Insight In1411 digital camera by means of a 200 mm MT1 tube lens from Edmund Optics (York, UK). This camera is based on a Kodak KAI-4021-M 2048 × 2048 pixel CCD sensor (Eastman Kodak Company, Rochester, NY, USA) with a pixel size of 7.4 μm and a saturation level of 27 300 electrons, leading to a signal-to-photon-noise ratio of about 160 at saturation. Images are acquired with a 14-bit A/D converter but are later processed in 8 bits after a linear renormalisation. The numerical aperture ensures an optical resolution (radius of Airy dots) close to 1 μm, consistent with the pixel size in the object space of 0.74 μm, the field of view being equal to 1.5 × 1.5 mm^2. Two lighting conditions can be adopted. The normal light made possible by a prism placed between the objective and the tube lens provides contrasted images in which the clay matrix appears almost black while the polished surfaces of the other mineral grains reflect a large amount of light. This brightfield observation mode gives access to the composite microstructure of the rock in the area under investigation. However, the almost uniform grey-level distribution in the matrix does not provide an appropriate contrast for DIC. That is

why an additional lateral lighting mode based on two 1-W high-power, white light-emitting diodes (LED) oriented at ∼45° with respect to the sample surface is used. It emphasises the contrast induced by the non-flat surface of the clay matrix, with a characteristic size of a few micrometres or less (see Figure 1). This provides a contrast with a rather wide grey-level distribution and a typical pattern size of several pixels in the matrix (see bottom of Figure 2), which is more suitable for DIC algorithms. However, this contrast is not as uniformly distributed in the image as would be a standard speckle painting. Furthermore, it is essentially based on shadows and reflections of light on the rough parts at the surface of the sample, which strongly depend on the relative geometric positions of the light source, the camera and the sample, and might not satisfy the condition of grey-level advection DIC algorithms are based on. Two procedures are adopted to limit the errors induced by possible evolutions of this geometry. First, the LEDs are mounted directly on the objective lens and, secondly, the microscope is moved during the mechanical test in such a way that a given detail at the centre of the image remains at the same pixel position. This is performed thanks to a hand-operated micrometric X–Y–Z stage on which the microscope is fixed and a continuous high frame rate display of the images on a monitor in front of the operator, who at the same time adjusts the Z-axis in order to compensate out-of-plane motions of the sample too (due essentially to Poisson's effect); this is required because of the very low depth of field (a few micrometres) induced by the high numerical aperture of the lens. Images are recorded only when they are focused and appropriately centred. The Spot software provided by the camera manufacturer allows such a procedure. In practice, it is possible to record a good image every 5 to 10 s (∼150 images per test). Developments are on, aiming at automating this camera-positioning procedure.

Image processing and post-processing

While pioneering applications of DIC date back to the 1980s [11], this technique is in the process of becoming a standard quantitative tool in experimental mechanics, at least at a macroscopic scale. More recent applications at a microscale, making use of SEM or OM images, are also reported [5, 8, 12–14]. We refer to Bornert *et al.* [15] for a review of various DIC formulations and their relative performances. The images obtained with the above-described optical devices are processed with the in-house Unix-based DIC software CMV [8, 10, 12]. The so-called 'zero-centred normalised cross-correlation coefficient', a local affine transformation of the correlation subsets and a bilinear interpolation of the grey levels of the deformed images (bicubic has also been tested but without significant evolution of the results), are used. Displacements are determined on a regular array of positions in a region of interest defined by the user. Note that the higher order terms of the local affine transformation are determined in an iterative way from the displacements of neighbour points of a particular position. At each iteration step, only translation components are optimised to subpixel accuracy, the higher order terms being kept constant and updated before the next iteration. Such an easy-to-implement procedure turns out to be more stable than a classical full optimisation, even if it might be slower and its spatial resolution slightly lower. It is suited to the considered images in which the local contrast might, in some subsets, not be sufficiently rich to fully identify higher order transformations accurately.

Once in-plane components of displacements are determined on a regular array of positions, deformations at various scales are computed making use of the procedures described by Allais *et al.* [7]. Without going into the detail, let us emphasise that the transformation gradient at a given position $\underline{X}$ in the reference image with component X_i and at a scale L, $\underline{\underline{F}}^L(\underline{X})$, with components $F^L_{ij}(\underline{X})$, is defined as the average transformation gradient on a domain $D(L,\underline{X})$ of size L, centred on $\underline{X}$, and depends only on the displacement field at the boundary of $D(L,\underline{X})$, according to Green's relation:

$$F^L_{ij}(\underline{X}) = \frac{1}{|D(L,\underline{X})|}\int_{D(L,\underline{X})}\frac{\partial x_i}{\partial X_j}(\underline{u})\mathrm{d}u = \frac{1}{|D(L,\underline{X})|}\int_{\partial D(L,\underline{X})} x_i(\underline{u})n_j(\underline{u})\mathrm{d}s_u \qquad (1)$$

where $|D(L,\underline{X})|$ is the measure of $D(L,\underline{X})$, $\partial D(L,\underline{X})$ its boundary with outer unit normal $\underline{n}$ and $\underline{x}(\underline{u})$ the position of $\underline{u}$ in the deformed image. Such a definition is consistent with general micro–macro relations [16]. When this general relation is specialised to 2D components, the integral on the right-hand side of Equation (1) reduces to a contour integral, which can be discretised on the set of measurement points, to obtain the relations given by Allais *et al.* [7]. Strain and rigid-body rotation components at the same scale L are obtained from $\underline{\underline{F}}^L(\underline{X})$ with classical relations. As small strains (below 5%) are considered in the present study, they reduce to their linearised version and in-plane strain components can be computed without out-of-plane displacement evalu-

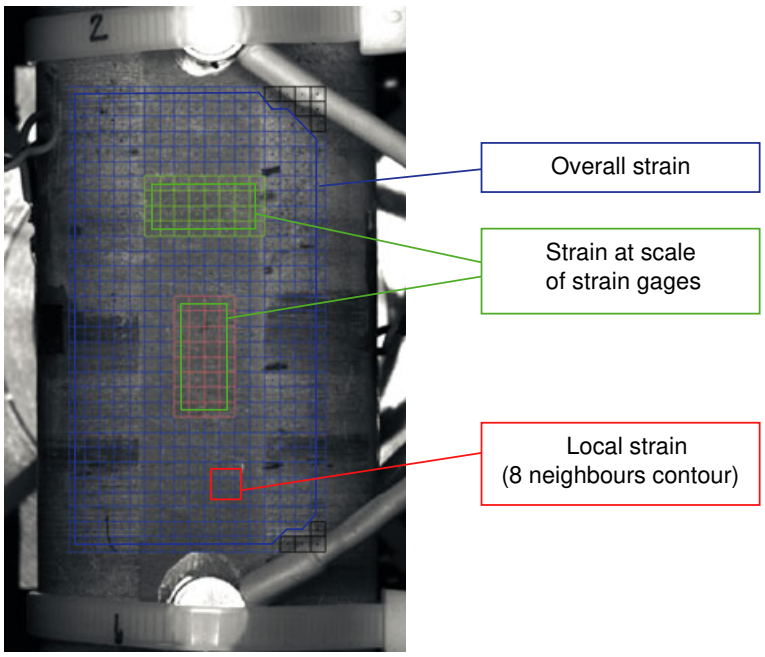

Figure 3: Example of discrete measurement positions on macroscopic images and of various averaging domains leading to strain evaluations at various scales. DIC subsets size is d = 30 pixels

ations. When *D* is the whole region of interest, one gets the overall strain components, which are comparable with the measurements obtained with the LVDT sensor in case of the macroscopic images (see Figure 3); when *D* is delimited by the eight first neighbours of a given measurement position, one gets the local gradient components considered in the present study (scheme 'c' in Figure 11 in Allais *et al.* [7]), associated with a local gauge length equal to twice the distance between two measurement positions. But any other averaging domain can be adopted, such as the centimetric surface of same size as the strain gauges, the obtained strain components being then comparable with the measurements obtained with these gauges.

Review and quantification of main experimental errors

Errors in 2D DIC measurements have various sources: image noise; local contrast evolutions; image-processing errors such as those induced by image interpolation or inadequate subset shape function [15]; or geometric errors induced by optical distortions or geometric evolutions of the setup (e.g. magnification fluctuations). While an exhaustive evaluation of

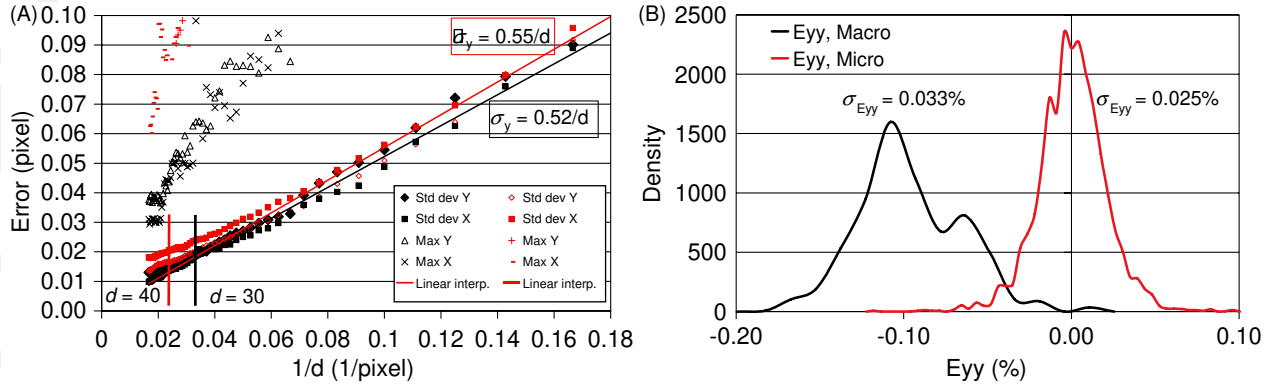

Figure 4: DIC measurements errors evaluated from rigid transformations: pure translation for MicroDIC (red curves) and out-of-plane translation leading to a magnification variation of 0.1% for MacroDIC (black curves). Dependence with subset size d of DIC error on displacement (A) and distribution of YY components of local strain using a d · d pixel subset and d pixels between two displacement measurements, d = 40 for MicroDIC and d = 30 for MacroDIC (B)

errors is a rather hard task and still an open question, indications on the accuracy of the measurements can be obtained from the analysis of rigid-body motions of the sample. More precisely, the displacement independently measured at a large number of positions can be compared with the theoretical displacement associated with an overall affine transformation (which is preferred to a rigid transformation because of possible out-of-plane motions and geometric imperfections of the optical setup) that best fits all measurements. Alternatively, statistical fluctuations of local strains, which should in principle vanish, provide an estimate of the errors on strain measurements, which can be considered as lower bounds for the actual errors because not all sources of errors are tested this way.

Figure 4A gives the evolution of the standard deviation of the X and Y displacement errors evaluated according to the first procedure as a function of subset size. A simple translation (*c.* −1.7 pixels in the X direction and 0.6 in the Y direction) and 1600 independent subsets were considered to obtain results for MicroDIC, and an out-of-plane motion inducing magnification variation of 0.10%, evaluated at 232 positions, for MacroDIC. Standard deviations of the displacement components are observed to depend almost linearly with the inverse of the subset size d, consistent with the analysis proposed by Besnard *et al.* [17] specialised to the particular case of rigid translation shape functions, MicroDIC errors being slightly larger. In the following, subset sizes of $d = 30$ or 40 pixels are used and lead to standard deviations σ_{u_i} below 0.02 pixels for such rigid or homogeneous transformations, i.e. 15 nm and 1 μm for MicroDIC and MacroDIC, respectively. Note however that maximal MicroDIC errors are significantly larger. It can be verified that these large errors correspond to subsets with very low contrast (inside large particles that appear uniformly black under lateral light) or with saturated pixels because of intense local light reflections. Such situations are easy to detect and can conveniently be removed manually from the region of interest through of the graphical user interface of the CMV software. The development of a procedure performing this task automatically was not considered necessary, as the number of such positions was rather low.

Errors on strain components are derived from those on displacements and depend on the gauge length and the number of independent displacement evaluation used. The general relations provided in Allais *et al.* [7] simplify into the following generic expression of their standard deviation

$$\sigma_{F_{ij}} = \alpha \frac{\sqrt{2}\sigma_{u_i}}{\sqrt{N}L_j} \tag{2}$$

where L_j is an equivalent gauge length along direction j, N is the number of pairs of independent displacement measurements used for the computation of the gradient F_{ij} and α is a coefficient close to 1, not detailed here. For local strain measurements, using $N = 3$ and $L = 2d$ (eight neighbours scheme), one gets $\sigma_{F_{ij}} \approx 0.03\%$ for MacroDIC with $d = 30$ (gauge length of 3 mm) and $\sigma_{F_{ij}} \approx 0.02\%$ for MicroDIC ($d = 40$, gauge length of 60 μm). These values are perfectly consistent with the strain distribution functions obtained with the second procedure for error evaluation and plotted in Figure 4B, which shows in addition that maximal errors can reach 0.05% for MicroDIC and 0.08% for MacroDIC. Errors are much smaller when larger gauge lengths are considered, and can go below 10 microstrains for the microscopic strain averaged over the whole region of interest (millimetric in size).

Note however that these evaluations do neither take into account the effect of possible evolutions of the local contrast, which are hard to evaluate, nor those due to imperfection or evolutions of the optical setup. Concerning the latter, one can evaluate the influence on MacroDIC measurements of variations of the magnification g because of out-of-plane motion by looking at the apparent deformations as a function of the Z displacement of the camera. One finds that it is perfectly consistent with a standard pinhole model, with an object to optical centre distance CO equal to 810 mm, i.e. $\Delta g/g = \Delta Z/\mathrm{CO}$. With a Poisson's ratio of $\nu = 0.5$ (it is actually lower) and a sample radius of $R = 18$ mm, the error on strain measurements because of transverse deformation is then $\Delta\varepsilon/\varepsilon = \nu R/\mathrm{CO} \approx 1\%$, which can be neglected. Such a problem does not occur with MicroDIC because of the very small depth of field (<4 μm) and the continuous focusing during the test. Magnification variations between both limits of the in-focus Z range are of the order of 0.05% and can also be neglected. Overall out-of-plane rotations of the sample can easily be detected with MicroDIC for the same reason. For MacroDIC, their effect on the strains measured on the flats is of second order with respect to the angle of rotation for simple geometric reasons and can also be neglected. It is of first order for strain components measured on the non-polished sides of the sample which are not perpendicular to the optical axis. Such rotations are thus easily detected by strain discontinuities at the borders of the flats, which have indeed been observed for compression tests along a direction at 45° with respect to the bedding plane (see Ref. [6] for more

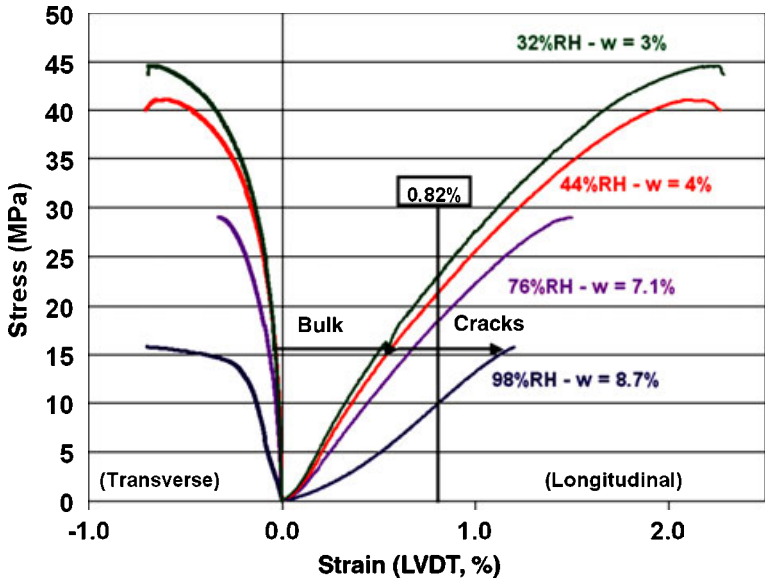

Figure 5: Overall stress–strain relations deduced from global LVDT strain measurements for the longitudinal strain, and strain gauges for the transverse strain, as a function of relative humidity and water content w. Probable decomposition of strain in wet samples (see section Selection of Results)

details), but not on the tests reported in the next section. Such geometric imperfections could have been avoided with a stereo-correlation setup at the macroscale, but as they are not critical at the considered deformation levels, such developments are left for further studies.

Selection of Results

These optical setups have been used on uniaxial compression tests on the Callovo-Oxfordian argillaceous rocks, for various water contents and compression directions with respect to the bedding plane. For brevity, only a short selection of results is given here, focused on a comparison between the multiscale mechanical response of an almost dry rock (44% RH) and that of an almost saturated one (98% RH). More exhaustive data can be found elsewhere [6]. Consider first the overall stress–strain relations given in Figure 5, in which the longitudinal strain is deduced from LVDT displacement measurements and the transverse strain from strain gauges.[1] The strong dependence on the water content is clearly evidenced, with a simultaneous decrease in ultimate stress, strain at failure and moduli when samples get wetter [1]. A shortcoming of the interpretation of these results could lead to the conclusion of a stronger ability of the water-sensitive clay matrix to deform plastically when its water content increases, together with a lower strength.

However, a more detailed analysis made possible by means of strain field measurements, first at the macroscopic scale, shows that the response of wet samples is much more heterogeneous, as seen on top of Figure 6, where equivalent strain[2] maps are plotted on both samples at the same overall strain. This shows that the difference in behaviour is connected with a new scale of heterogeneity, centimetric in size, much larger than that of the mineral inclusions already described. This is confirmed by the plots at the bottom of Figure 6, where overall stress–local longitudinal and transverse strain curves are plotted for various averaging domains. They confirm first the homogeneity of the strain in the dry sample all along the loading history, and the consistency between MacroDIC measurements and more classical LVDT and strain gauge data. The small discrepancy with the LVDT at the beginning of the curve can be related to the squashing of the interfaces between the sample and the test machine; one can also notice the failure of the longitudinal strain gauge at ∼1%. This similarity of all curves confirms that the test is indeed representative of an intrinsic property of the material, which is further confirmed by the identity of the overall response of three other samples tested with only classical macroscopic strain measurements. This is definitively not the case with the wet sample, on

[1]Note that rock mechanics conventions are used: stress and strains are positive in compression and contraction, respectively.

[2]Defined as $E_{eq} = 2(E_1 - E_2)/3$, where $E_1 > E_2$ are the principal in-plane strains, such that E_{eq} is equal to the longitudinal strain in case of an axial symmetric isochoric deformation (i.e. purely deviatoric strain).

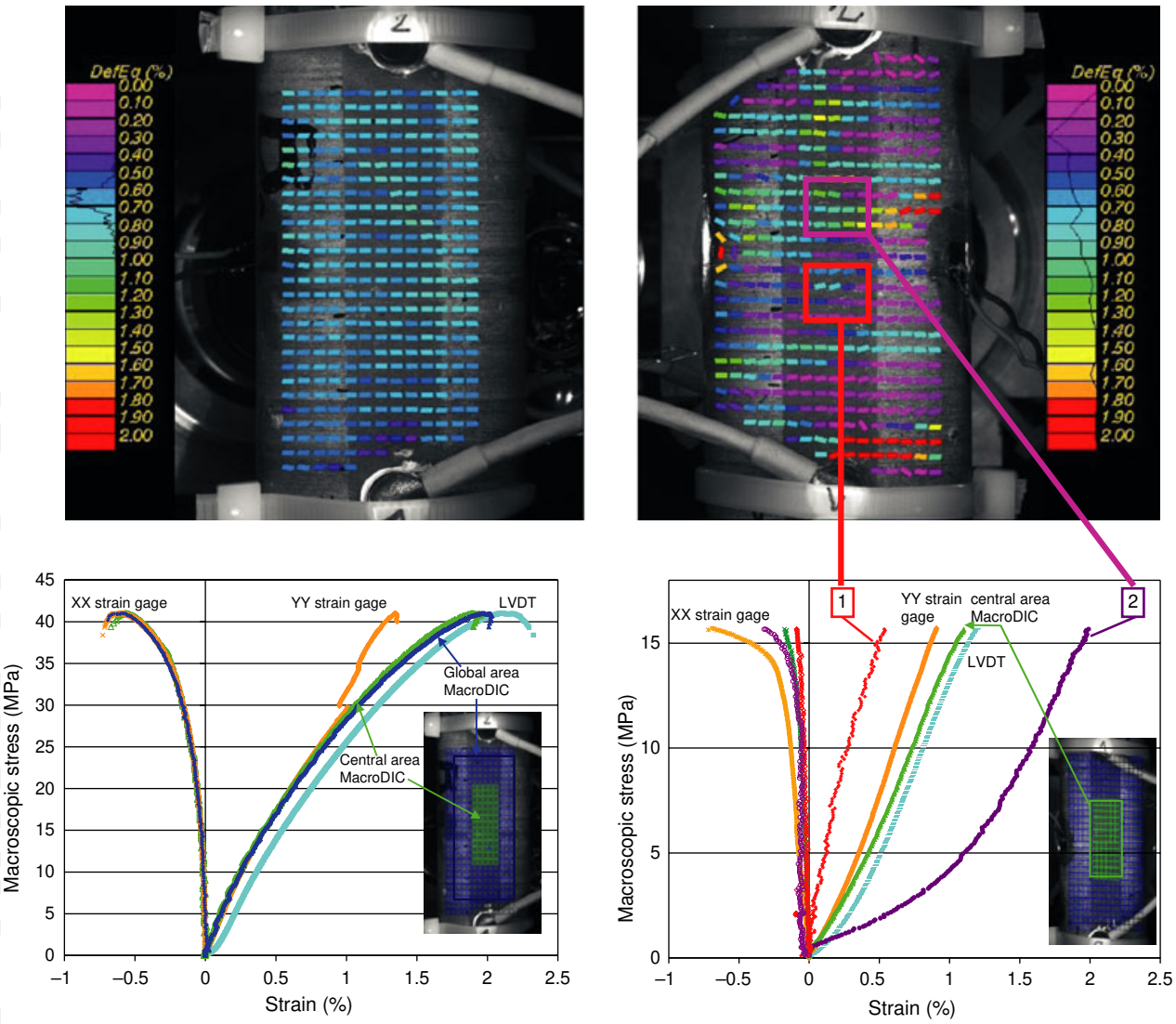

Figure 6: Comparison between 44% RH (left) and 98% RH (right) samples at the macroscopic scale. Top: colour map of the second invariant of strain field at the same level of overall compression strain (E_{YY} = 0.82%, vertical line in Figure 5), symbols are oriented along the principal axis, strain distribution functions are superimposed on the colour maps. Bottom: apparent stress–strain relations obtained with various averaging zones

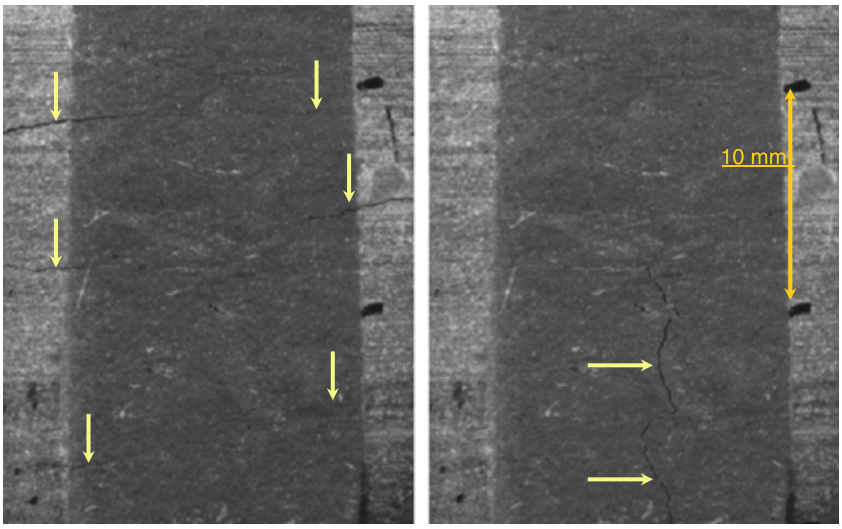

Figure 7: Same zone of wet pre-cracked sample before (left) and under (right) load, just before failure; transverse cracks closings and longitudinal cracks opening

which every averaging domain generates a different result. This strong heterogeneity is clearly related to the presence of the pre-existing cracks, which have appeared during the suction, as mentioned at the end of the section, *Materials and General Experimental Methodology*. Figure 7 is a zoom on an area with several longitudinal hydric cracks that close during the compression test and a transverse crack that opens. A more detailed observation shows that the network is rather complex, the crack length being comparable with the diameter of the sample, with a maximal opening of the order of 10 μm and a typical spacing of a few millimetres. When one measures the strain on a 5×5 mm^2 area that fits in between two cracks, such as area 1 in the right-hand side of Figure 6, thus avoiding to take into account the contribution of the cracks, one finds a strain level that is more or less half the overall measured strain (red curve to be compared with cyan curve). Assuming the local stress in such an area to be close to the overall stress,[3] the resulting stress–strain curve for such a wet, but undamaged, area would be very close to that of the dry samples (see horizontal line on Figure 5). The apparent overall soft behaviour of the wet sample is thus clearly a consequence of the presence of this network of cracks and not a consequence of an evolution of the physical properties of the clay matrix.

This is confirmed by the analysis at the microscale, from which additional information can be extracted. As all millimetric areas are equivalent on the dry sample, since they deform similarly as shown by MacroDIC, the microscope can be placed randomly on the polished flat of the sample. This is not true for the wet sample, for which different behaviour might be expected, depending on the macroscopic level of strain in the surroundings of the field of view of the microscope. The choice has been made to focus the local analysis on the neighbourhood of a small pre-existing crack, placed at the upper right of the 1.5×1.5 mm^2 field of the microscope. Figure 8 shows the obtained strain maps as well as the overall stress–local strain curves obtained with various averaging zones. First, it is observed that the strain average over the whole investigated area on the dry sample coincides with the macroscopic measurements, confirming that this area is again representative, in terms of deformation, of the material. But unlike at the macroscale, the strain field is now strongly heterogeneous because of the composite structure of the rock, with a clear correlation between local deformation level and dominant constitutive phase in the local averaging area (45×45 μm^2 in that case). The clay matrix deforms much more than the other mineral grains, but it also appears that the deformation is very inhomogeneous in the matrix, with some areas almost not deformed, while others exhibit deformation twice the overall strain, depending on the local distribution of the inclusions. Such quantitative information might be extremely useful for the development of micromechanical models for such material, in order to validate them in terms of predictions at the scale of the constitutive phases. It permits in addition to determine a typical size of a volume element which is representative of the material in terms of deformation. Indeed, when one computes local strains on domains of various sizes L and performs a statistical analysis over randomly placed positions in the form of strain distribution functions, as in Figure 9, one finds that averages over sizes larger than about 700 μm generate almost uniform fields (less than 5% fluctuations from one value to another), which suggests that this rock can be considered as a homogeneous material at scales above this value and for this particular physical state.[4]

This is of course not the case for the wet sample for which the macroheterogeneous behaviour has already been evidenced. The local analysis in the neighbourhood of the crack shows an additional scale of heterogeneity. Indeed, the strain map on Figure 8 shows clearly two zones: a first one, up to a distance of about 500 μm from the crack, where the deformation levels are much larger, corresponding to a response of the material much 'softer' than that of the other zone farther away. In the latter, the characteristic lengths of the heterogeneities are correlated with the microstructure and very similar to those in the dry sample, suggesting a very similar behaviour. This is quantitatively confirmed by, first, the plot on Figure 10 which shows that for a given macroscopic stress, the deformation in this area is almost identical to the macrohomogeneous deformation in the dry sample, and, secondly, by the normalised strain distribution function for $L = 45$ μm, which is also identical to that of the dry sample (see Figure 9), confirming the observation made from the MacroDIC analysis that some parts of the wet sample behave as if they would not have been affected by the suction, and can be considered as 'sound' rock. The softer and weaker properties of the wet sample are thus essentially induced by the presence of the network of cracks, and a small surrounding area in

[3]This is an approximation, but probably not so far from reality, as global equilibrium ensures that the average stress is constant in any transverse section of the sample, in particular those delimited by the subhorizontal cracks.

[4]However, note that this is not a general result; macroscopic heterogeneities linked to spatial variations of the proportions of the constitutive phases have been observed in other samples [5].

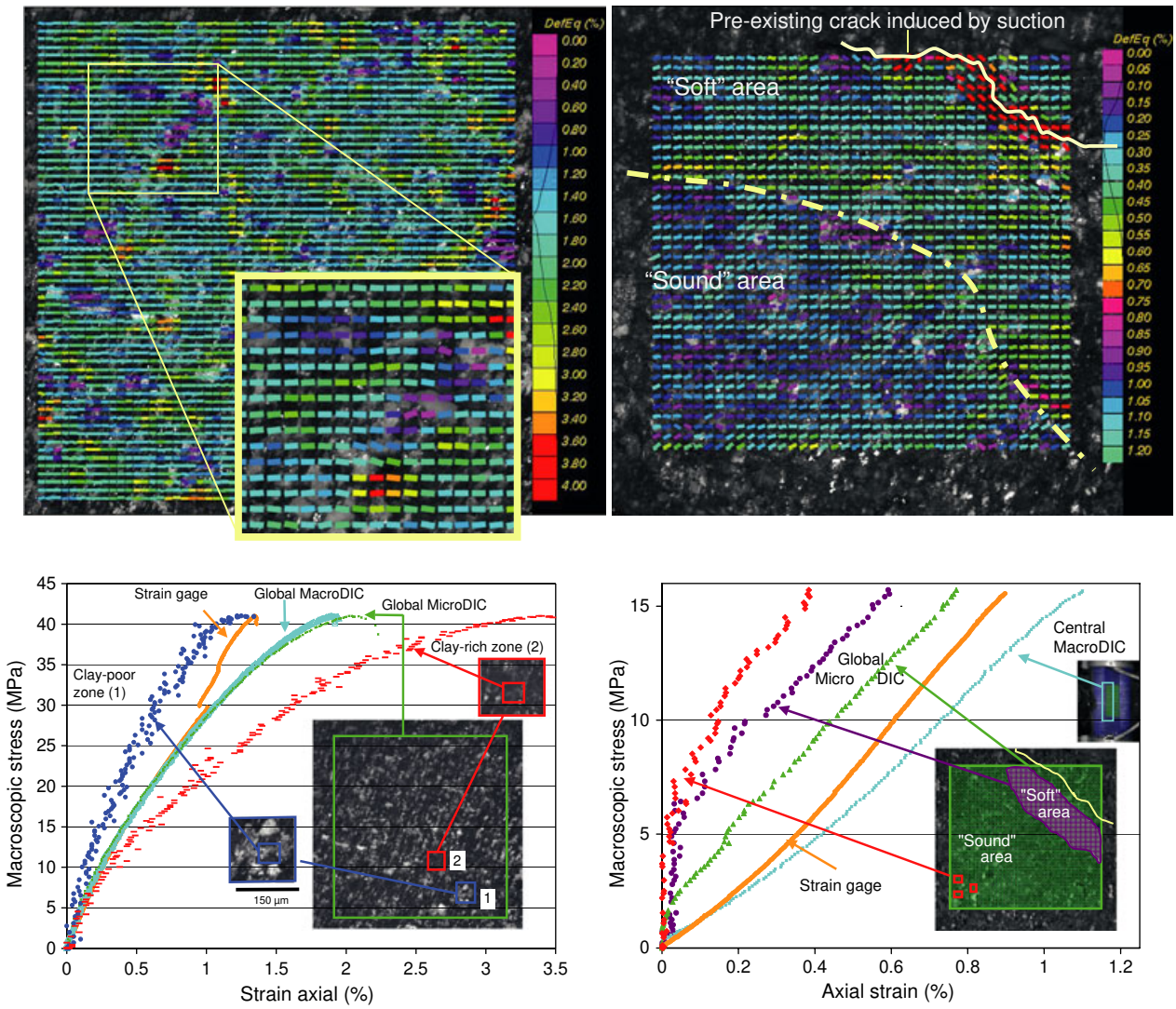

Figure 8: Comparison between 44% RH (left) and 98% RH (right) samples at the microscopic scale. Top: colour map of the second invariant of strain field a few steps before the failure of the sample, local gauge length is 45 lm (d = 30 pixels) for the dry sample and 60 lm (d = 40 pixels) for the wet sample, field width is 1.5 mm in both images. Fields are superimposed on the OM images obtained with normal lighting conditions, which emphasise the composite structure. Bottom: global stress – local/averaged strain relations: local strain at clay-poor (position 1) and clay-rich (position 2) zones and overall strain on the dry sample; average over 3 positions (red) far away from the crack, average on the blue zone near the crack, average over whole MicroDIC zone and central average on MacroDIC

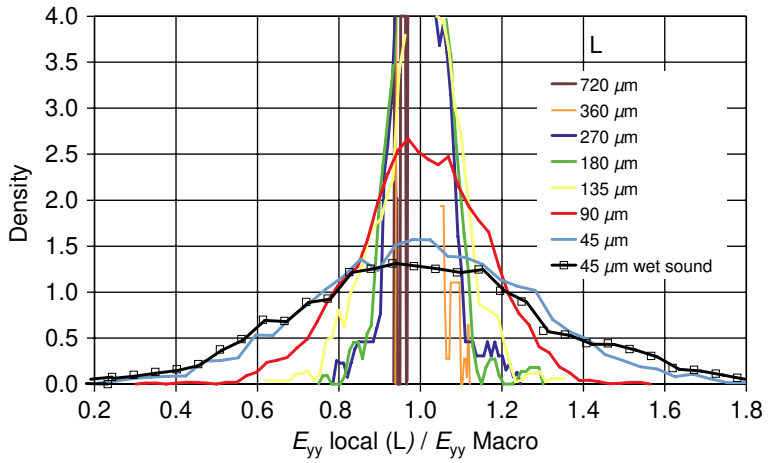

Figure 9: Strain distribution functions in the dry sample deduced from the MicroDIC measurements, for various gauge lengths L (obtained by considering domains D of size L · L to compute local strains). Overall strain is E_{YY} = 2.0%. Distriribution function for the sound zone of the wet sample for L = 4 5 lm is superimposed; average compression on this zone is 0.27%

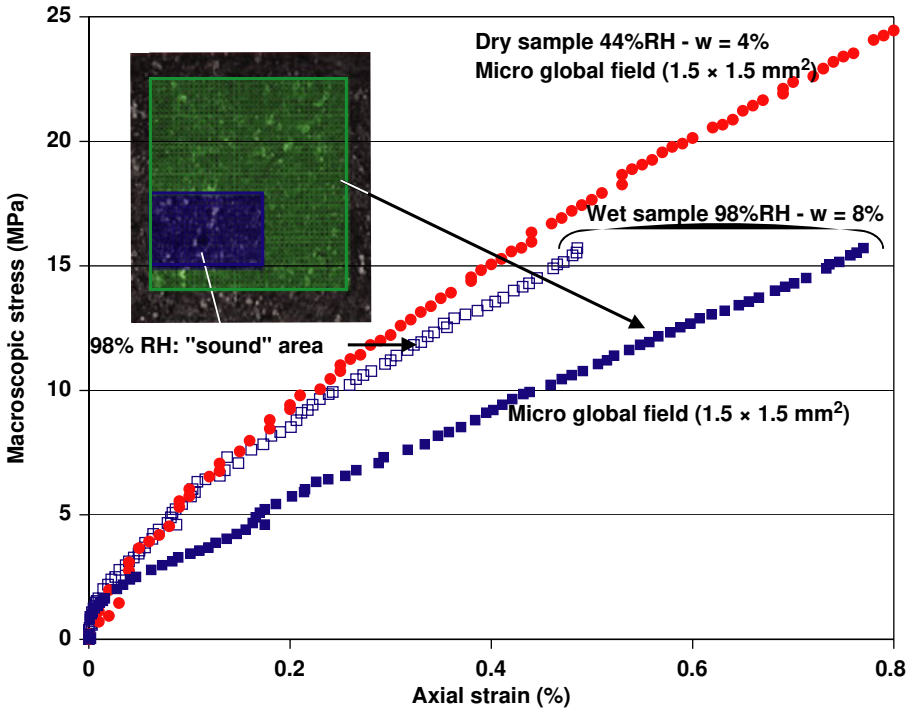

Figure 10: Overall stress–average longitudinal strain curves obtained from MicroDIC analysis. Strain is averaged over the whole (representative) field of view for the dry sample, and both on the whole field and an area in the 'sound' zone for the wet sample

which the rock undergoes much larger deformations. The physical origins of these larger deformation levels are unclear at this stage. They might be linked with locally different compositions of the clay matrix, the existence of privileged paths for the transport of water in the rock, or they might simply be the sign of a local diffuse damage at a smaller scale in the matrix, induced by the motion of the nearby crack (process zone). The latter assumption would be consistent with the fact that acoustic emissions are recorded from the beginning of the test on the wet sample, and their localisation coincides with cracks, while dry samples do not emit almost any signal up to 70% of their stress at failure [6].

Conclusions and Perspectives

Digital image correlation techniques have been shown to be an efficient tool for the multiscale analysis of the hydromechanical behaviour of clayey rocks. The natural contrast at various scales can be used as local markers for the evaluation of displacements. Results show that the softer response of wet samples is essentially governed by the presence and the motion of cracks induced by the preliminary swelling, the intrinsic behaviour of the sound rock being almost unchanged with respect to dry materials. The characteristic scale of this network of cracks is similar to the size of the samples and strain gauges used for the overall investigations. This explains the rather large variability observed on the overall response of the three wet samples that have been tested, which can thus not be considered as fully representative of the behaviour of the damaged wet materials. This differs from the very reproducible behaviour of dry samples, for which the size of the representative surface can be shown to be of the order of 1 mm. This illustrates the appropriateness of full-field measurement techniques for the detection of characteristic scales of heterogeneities and the validation or the proper interpretation of classical mechanical tests. In addition, the quantification of the heterogeneity of the deformation at the scale of the composite structure is useful for the development and validation of multiscale constitutive models for such materials. However, the spatial resolution of the presented technique is not sufficient for a clear separation of the contribution of each constituent. Similar analysis at a smaller scale might be performed, making use of recent developments in environmental SEM and *in situ* testing in such devices [18]. Additional investigations will also be required for a better understanding of the crack generation during the swelling process as well as for the multiscale analysis of the long-term deformation of these rocks (creep), again as a function of the water content. Towards that purpose, an environmental chamber allowing a continuous monitoring of the sample at various scales is currently under development. As the behaviour of such rocks is also strongly dependent on their confinement, triaxial tests with

continuous imaging for instance by means of computed X-ray tomography will also be required, both to characterise the generated network of cracks and to evaluate the local deformation in the sample by volumetric DIC techniques [10].

ACKNOWLEDGEMENTS

We wish to thank ANDRA for financially supporting this project and for supplying core samples from the site at Bure, France, as well as CNRS for its additional financial support (ATIP research program). SEM images of the microstructure in Figure 1 were obtained with the help of D. Caldemaison from LMS, on the environmental SEM FEI Quanta 600 which has been acquired with the financial support of Region Île de France (SESAME 2004 program), CNRS and École Polytechnique.

REFERENCES

1. Valès, F., Nguyen Minh, D., Gharbi, H. and Rejeb, A. (2004) Experimental study of the influence of the degree of saturation on physical and mechanical properties in Tournemire shale (France). *Appl. Clay Sci.* **26**, 197–207.
2. Dormieux, L., Lemarchand, E. and Sanahuja, J. (2006) Macroscopic behavior of porous materials with lamellar microstructure. *C. R. Mecanique* **334**, 304–310.
3. Abou-Chakra Guéry, A., Cormery, F. and Kondo, D. (2007) Modélisation micro-macro du comportement élastoplastique endommageable de l'argilite du Callovo-Oxfordien. Proc. 18ème Congrès Français de Mécanique, Grenoble, France (available at: http://hdl.handle.net/2042/15826).
4. Gaucher, E., Robelin, C., Matray, J. M., Négrel, G., Gros, Y., Heitz, J. F., Vinsot, A., Rebours, H., Cassagnabère, A. and Bouchet, A. (2004) ANDRA underground research laboratory: interpretation of the mineralogical and geochemical data acquired in the Callovian–Oxfordian formation by investigative drilling. *Phys. Chem. Earth* **29**, 55–77.
5. Bornert, M., Eytard, J. C. and Valès, F. (2000) *Macro et méso-hétérogénéités de déformation dans une argilite*. ANDRA Internal Report, 25 pp.
6. Valès, F. (2008) *Modes de déformation et d'endommagement de roches argileuses profondes sous sollicitations hydro-mécaniques*. PhD dissertation, École Polytechnique, Palaiseau.
7. Allais, L., Bornert, M., Bretheau, T. and Caldemaison, D. (1994) Experimental characterization of the local strain field in a heterogeneous elastoplastic materials. *Acta Metall. Mater.* **42**, 3865–3880.
8. Héripré, E., Dexet, M., Crépin, J., Gélébart, L., Roos, A., Bornert, M. and Caldemaison, D. (2007) Coupling between experimental measurements and polycrystal finite element calculations for micromechanical study of metallic materials. *Int. J. Plasticity* **23**, 1512–1539.
9. Delage, P., Howat, M. D. and Cui, Y. J. (1998) The relationship between suction and swelling properties in a heavily compacted unsaturated clay. *Eng. Geol.* **50**, 31–48.
10. Lenoir, N., Bornert, M., Desrues, J., Besuelle, P. and Viggiani, G. (2007) Volumetric digital image correlation applied to X-ray microtomography images from triaxial compression tests on argillaceous rock. *Strain* **43**, 193–205.
11. Chu, T., Ranson, W., Sutton, M. and Peters, W. (1985) Applications of the digital-image-correlation techniques to experimental mechanics. *Exp. Mech.* **25**, 232–244.
12. Soppa, E., Doumalin, P., Binkele, P., Wiesendanger, T., Bornert, M. and Schmauder, S. (2001) Experimental and numerical characterisation of in-plane deformation in two-phase materials. *Comput. Mater. Sci.* **21**, 261–275.
13. Schreier, H. W., Garcia, D. and Sutton, M. A. (2004) Advances in light microscope stereo vision. *Exp. Mech.* **44**, 278–288.
14. Nguyen, Q. T., Millard, A., Caré, S., L'Hostis, V. and Berthaud, Y. (2006) Fracture of concrete caused by the reinforcement corrosion products. *J. Phys. IV* **136**, 109–120.
15. Bornert, M., Brémand, F., Doumalin, P., Dupré, J. C., Fazzini, M., Grédiac, M., Hild, F., Mistou, S., Molimard, J., Orteu, J. J., Robert, L., Surrel, Y., Vacher, P. and Wattrisse, W. (2009) Assessment of Digital Image Correlation measurement errors: methodology and results. *Exp. Mech.* (in press).
16. Hill, R. (1972) On constitutive macro-variables for heterogeneous solids at finite strain. *Proc. R. Soc. London* **326**, 131–147.
17. Besnard, G., Hild, F. and Roux, S. (2006) 'Finite Element' displacement fields analysis from digital images: application to Portevin-Le Châtelier bands. *Exp. Mech.* **46**, 789–803.
18. Sorgi, C. and De Gennaro, V. (2007) Analyse microstructurale au MEB environnemental d'une craie soumise à chargement hydrique et mécanique. *C.R. Geosci.* **339**, 468–481.